Proceedings World Geothermal Congress 2020+1
Reykjavik, Iceland, April - October 2021

# Hydrothermal Alteration Mapping using ASTER Image of Arta, Geothermal Area of Djibouti

Samatar Abdi[1,3], Tatsuya Wakeyama[2], Yasuhiro Fujimitsu[2], Jun Nishijima[2]

[1]Department of earth resources engineering, Graduate school of engineering, Kyushu university, Japan

[2] Department of earth resources engineering, faculty of engineering, Kyushu university, Japan

[3] Djiboutian office for geothermal energy development (ODDEG)

E-mail address: ratamas01@gmail.com

**Keywords:** ASTER, Hydrothermal alteration, Arta, geothermal exploration.

## ABSTRACT

Remote sensing plays an important role in geothermal exploration. It can be applied to recognize hydrothermal alteration, which is the first step in geothermal exploration. The main purpose of this study is to validate the ASTER images efficiency in the mapping of hydrothermal alteration in order to elaborate the image processing to be adequate to Arta which our study area. The perspective of this study is to be able to apply mapping technics and geothermal development. The ASTER L3A which covers the whole study area has been used. The image was correct by using the FLAASH algorithm. The performance of RGB image composite and band ratio (BR) has been evaluated. The RGB image composite on the resultant has highlighted the hydrothermal alterations. The Aster band ratio (BR) 3/2 and 4/3 enabled us to map the spatial distribution of vegetation and Iron oxide respectively in the study area. Principal compound analysis has been used to confirm the alteration mineral. The study area present hydrothermal alteration related to rhyolite intrusion. Results indicate that Aster is able to provide the hydrothermal alteration which plays an important role in geothermal exploration.

## 1. INTRODUCTION

The geothermal area is first detected in remote sensing technics by identifying Thermal anomalies (Hot spring and fumarole) and hydrothermal alteration. This Remote sensing technics can provide the information of distribution of altered mineral in the area which can help us to have information on the area before the visit. The altered mineral was generated by hydrothermal fluid processes which can alter the mineralogy and chemical composition (Amin B P et al., 2011). The Advanced Space borne Thermal Emission and Reflection Radiometer (ASTER) is a multispectral imager that was launched onboard NASA's Terra spacecraft in December, 1999 which covers the visible, near-infrared (VNIR), short wave infrared (SWIR), and thermal infrared (TIR) spectral regions with 14 channels with high spatial, spectral and radiometric resolution (Yamaguchi Y et al.,1998). Aster subsystem VNIR and subsystem SWIR can detect Iron mineralogy and Hydroxyl bearing such as clay mineral. By procession of subsystem (VNIR and SWIR) technics, we can detect the hydrothermal alteration exposition of Arta, study area. Arta area presents many geothermal manifestations (Fumarole) and hydrothermal alteration is very interesting because it is located in a very active zone (divergence system) featured by the rhyolite intrusion. The aim of the study is to use Aster data to map the alteration minerals zones related to the geothermal system in Arta.The alteration information associated with the geothermal area was extracted by using band ratio (BR) method, false Color composite (FCC) and principal compound analyze.

## 2. GEOLOGY SETTING

The Arta Geothermal field is located on a broad valley lying on the Gulf of Tadjoura approximately 30 km east of the Djibouti City. The area has an elevation of 0 m to about 720 m dissecting the ragged hills on both side along the access road.Figure 1 presents the geological map of Arta (Geological map of Tadjoura, 1985). Dalha basalt (9-4 Ma) is dominant, geographically from the Arta plateau to the Gulf of Aden.Dalha basalts are exposed in almost all of the area of the Arta geothermal field, from the Arta plateau to the Gulf of Aden and small rhyolitic intrusion-pyroclastic and its extensional to NNE trend fault systems are observed in the western half. It is a relatively well-dissected by lava plateau with successive fluvial sediments in their valleys. The fumarole point and alteration zone are located on the edge of wadi which is widely eroded. The mountains around are deeply dissected showing older topographic characteristics.

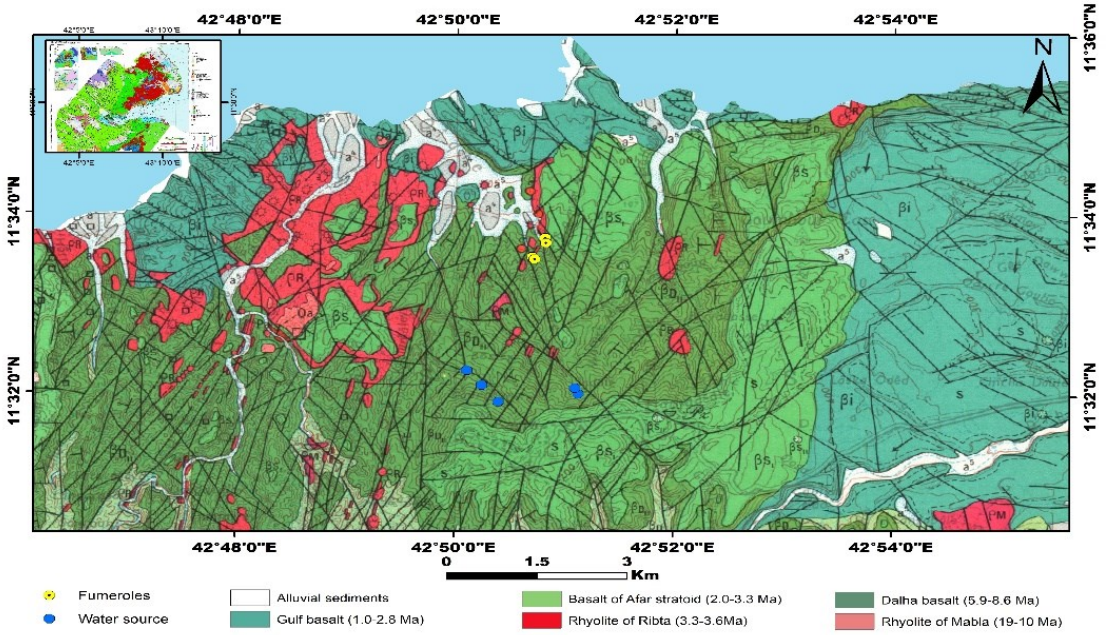


**Figure 1: Geological map of Arta.**

### 3. MATERIALS AND METHOD

In this study, the ASTER image was selected to detect the hydrothermal alteration. ASTER image is composite by three subsystems which represent in total 14 band. It measures reflected radiation in 3 bands between 0.52 and 0.86 µm (VNIR); in 6 bands from1.6 to 2.43 µm (SWIR); and emitted radiation in 5 bands in the 8.125- to 11.65-µm wavelength region (TIR) with 15-m, 30-m, and 90-m resolution, respectively (Fujisada et al., 1995) (Table 1). The image Aster L3A was used in this study. This image was acquired on June 12 ,2005. The pre-processing, carried out using the ENVI 5.3 software. All image 9 bands (VNIR & SWIR) were resampled to get the same size of pixels 15 x 15 meter. Atmosphere correction was applied by using Fast Line-of-sigth Atmospheric algorithm (FLAASH) to convert radiance at the sensor to reflectance and then followed by Minimum noise fraction (MNF) to reduce the noise on the image. After the pre-procession, the image was applied some procession methods such as colors composite, Band ratio, and principle compound analysis to provide the alteration mineral in the respective area.

**Table 1: Characteristics of 3 ASTER system**

| Subsystem | Band No. | Spectral Range (µm) | Spatial Resolution, m | Quantization Levels |
|---|---|---|---|---|
| 1 | 0.52-0.60 | VNIR | 15 | 8 bits |
| 2 | 0.63-0.69 | | | |
| 3N | 0.78-0.86 | | | |
| 3B | 0.78-0.86 | | | |
| 4 | 1.60-1.70 | SWIR | 30 | 8 bits |
| 5 | 2.145-2.185 | | | |
| 6 | 2.185-2.225 | | | |
| 7 | 2.235-2.285 | | | |
| 8 | 2.295-2.365 | | | |
| 9 | 2.360-2.430 | | | |
| 10 | 8.125-8.475 | TIR | 90 | 12 bits |
| 11 | 8.475-8.825 | | | |
| 12 | 8.925-9.275 | | | |
| 13 | 10.25-10.95 | | | |
| 14 | 10.95-11.65 | | | |

Source : ASTER Users Handbook (Version 2)

## 4. PROCESSION

### 4.1. Color composite

The color composite is a technic used to map lithology and mineral exploration. This method used the combination of three bands to create a colorful multispectral image respectively red, green and blue. According to the propose, this technic can be divide in to two sub-method: true-color composite (TCC) end false-color composite (FCC). The true color can provide nature colored of materials (vegetation green color, Water blue or Dark color and soil grey color).At the first to have an idea of the area, the true color composite has been select to emphases the vegetation, soil, and water (Figure 2).The false-color composite technics have been choose to map the lithology and hydrothermal alterations. The False-color composite image RGB (731) was select to discriminate the different lithology of the area (figure 3). For the hydrothermal alteration alteration, the false-color composite RGB (468) has been used to detect the different alteration present in the area (figure 4).

### 4.2. Band ratio

Band ratio (BR) is a technique where the Digital Number (DN) value of one band is divided by the DN value of another band. BRs are very useful for highlighting certain features or materials that cannot be seen in the raw bands (Inzana et al., 2003).The VNIR subsystem (band 1, band 2 and band 3) used to detect the Iron mineralogy and vegetation due to the wavelength range. The iron oxide such us (hematite, goethite and jarosite) can be detected using band ratio (b4/b2) because the iron oxide presents high reflectance band 4 and High absorption band 2(figure 5) (Volesky et al., 2003).The vegetation presented high absorption in band 3 and high reflectance band 2.The band ratio (b3/b2) used to identify the vegetation area (figure 6)(Roman et al 2003).The SWIR subsystem (band 4 to band 9) employed to identify the OH bearing and clay minerals such alunite ,kaolinite. In order to detect the OH bearing mineral, Ninomiya index has been used for the first OH bearing ((b4*b7)/(b6/b6)) and for the second OH bearing ((b4*b7)/(b5*b5)) (figure 7) ( Ninomiya et al., 2003a).

### 4.3. Principal compound analysis

Principal Component Analysis (PCA) is a multivariate statistical technique that selects uncorrelated linear combinations (eigenvector loadings) of variables in such a way that each component successively extracted linear combination and has a smaller variance (Singh and Harrison, 1985; Chang et al., 2006).Standard PCA transformation has been employed to the study area (Arta). The original raw data of nine-band (VNIR and SWIR) has generated nine new band image flowing by the statistics eigenvector matrix of nine bands (table 2).

## 5. RESULT AND INTERPRETATION

### 5.1. Color composite

The color composite was applied in order to analyze the study area. The ASTER color composite was able to produce the different band combinations, some of them enhancing the lithology and hydrothermal alteration. The true color composite RGB (B2, (B1*3+B3)/4 , B1) highlight the vegetation in green, the water in blue and soil grey.This true-color composite gives us an idea about the vegetation distribution and water which are very important when we deal with hydrothermal alteration. Indeed, the vegetation presents a bit similar wavelength with the alteration (iron). The vegetation can interfere with the alteration and same case the alteration became difficult to identify due to the high dense vegetation. According to the true color composite (figure 2), the study presents very few vegetation (negligible).On the other hand, the water body is absent in the area. The false-color composite RGB (B7, B3, B1) was useful to describe the lithology unite and alteration. For false-color composite RGB (B7, B3, B1), the rhyolite unite is indicated green to blue color and the basaltic unite is indicate red color. On the other hand, the argillic alteration, phyllic alteration indicate us green to blue color and porphyritic alteration represent red color (figure 3).The false-color composite RGB (B4, B6, B8) were generated to map hydrothermal alteration. This false-color composite us the best false color combinations. This FCC identify the advance argillic alteration (alunite, kaolinite) and phyllic alteration (sericite,smectite) are indicated red to pink color, Propylitic alteration (chlorite,epidote ) is indicated in pale green and calcareous unite appears yellow. The advance argillic alteration (alunite, kaolinite) and phyllic alteration (sericite, smectite) both of them have high absorption at band 6, low reflectance at band 8, high reflectance at band 4 (Figure 4 ). Propylitic alteration (chlorite, epidote) has absorption at band 8 cause by Mg-OH, broad absorption at band 4 caused by iron in chlorite or epidote, no absorption at band 6 (Fig 4). Calcite has absorption at band 8 caused by C03 but does not absorption at band 4 because calcite lacks iron and no absorption at band 6.

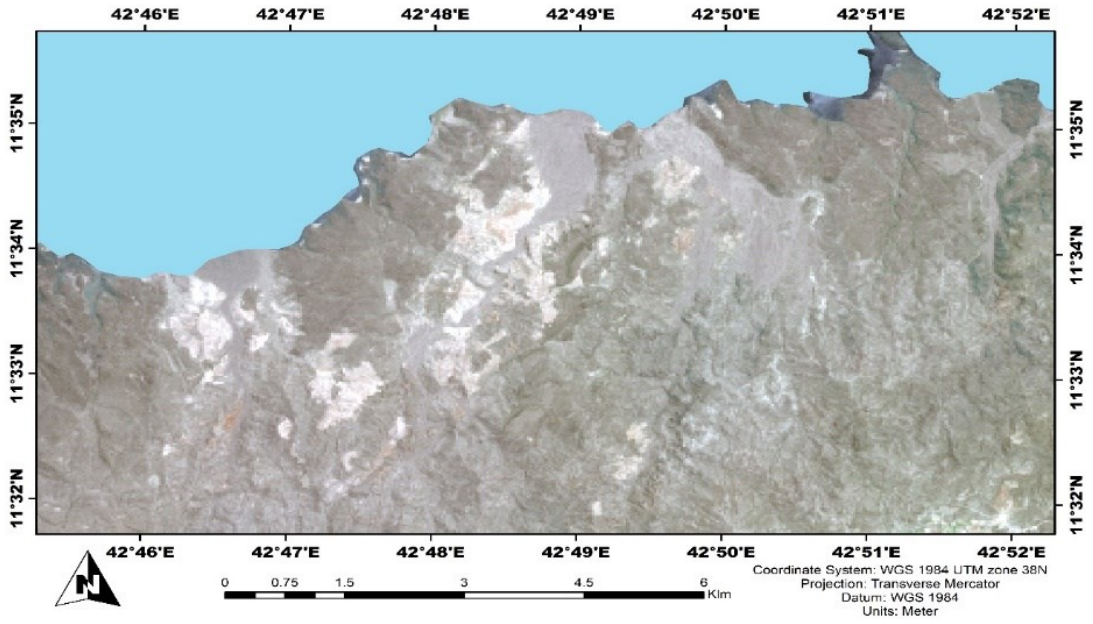


**Figure 2: ASTER true color composite (R:G:B = B2 , (B1*3+B3)/4 , B1)).**

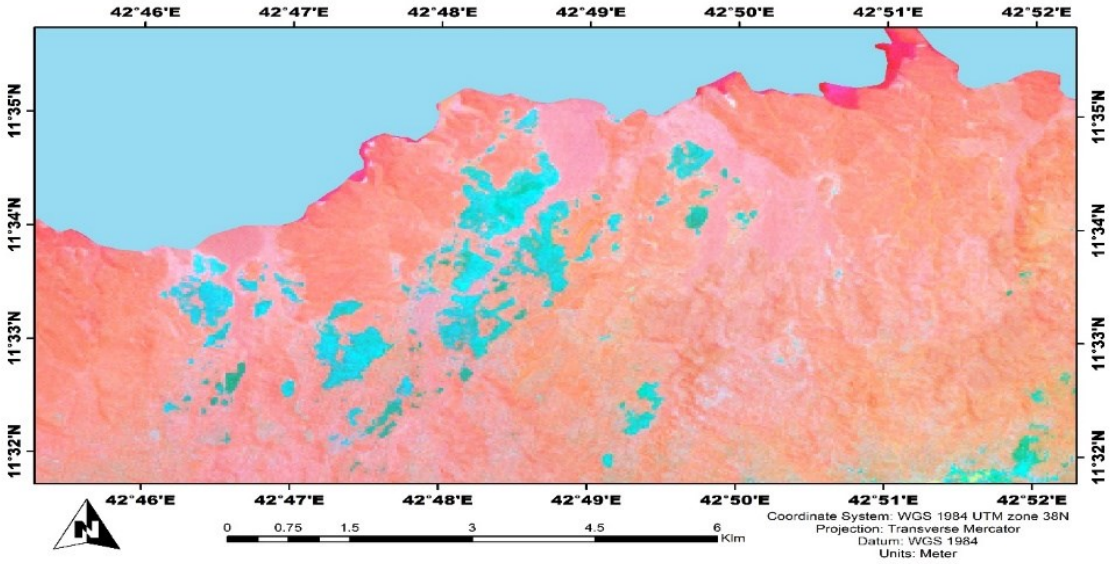


**Figure 3: ASTER false color image (R:G:B =band 7:band 3: band 1), Red: basaltic unite,Green to cyan: Rhyolite unite , Magenta: sediments unite.**

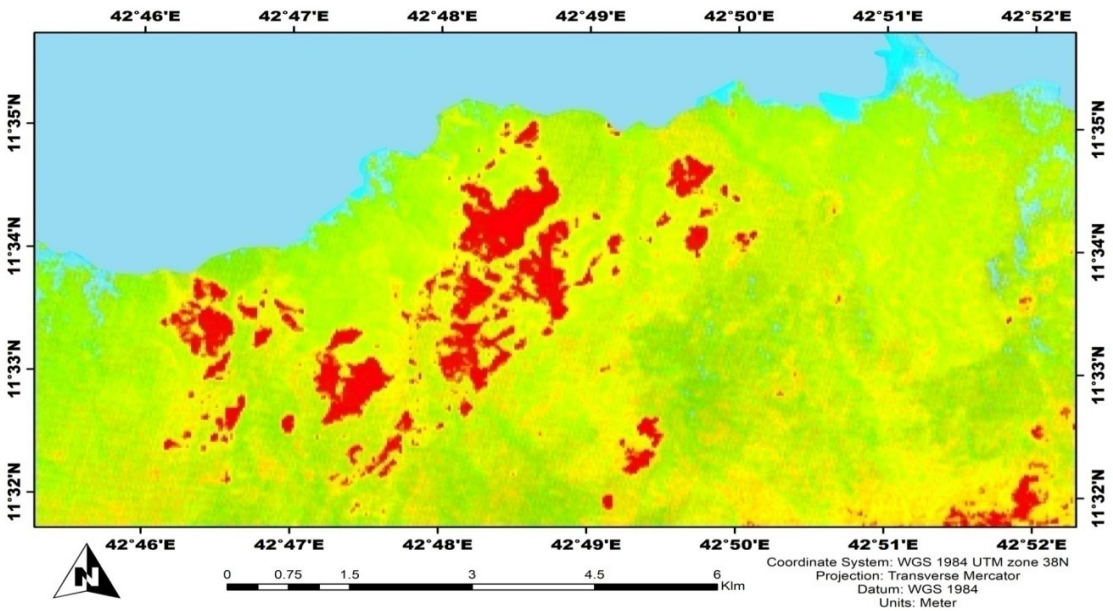


**Figure 4: ASTER SWIR false color image (R:G:B =band 4:band 6: band 8), Red to pink : advanced argillic and phyllic alteration, Pale green:propylitic alteration , Yellow : calcareous units.**

### 5.2. Band ratio

The band ratio was emphases to map the alteration area specially the iron oxide and hydroxyl bearing. The band ratio (b4/b2) were generated to map the iron oxide respectively and (Volesky et al., 2003) because the iron oxide has a high reflectance to band 4 and low reflectance to band 2. The iron oxide appears as bright pixel, that region corresponds to the basaltic unite(Figure 5).The vegetation was highlight using band ratio (b3/b2) due to the high reflectance in band 3 and low reflectance in band 3 (Xu et,. 2004). The vegetation appears as bright pixel (figure 6).The first hydroxyl bearing ($OHI_a$) such as montmorillonite and Mica have been detected by using band ratio ((b4*b7)/(b6/b6)) with has a deep and sharp absorption feature at ASTER band 6 .The second hydroxy group ($OHI_b$) has shown the distribution of propylitic alteration by using band ratio ((b4*b7)/(b5*b5)) (figure 7) (Ninomiya et al., 2003a).

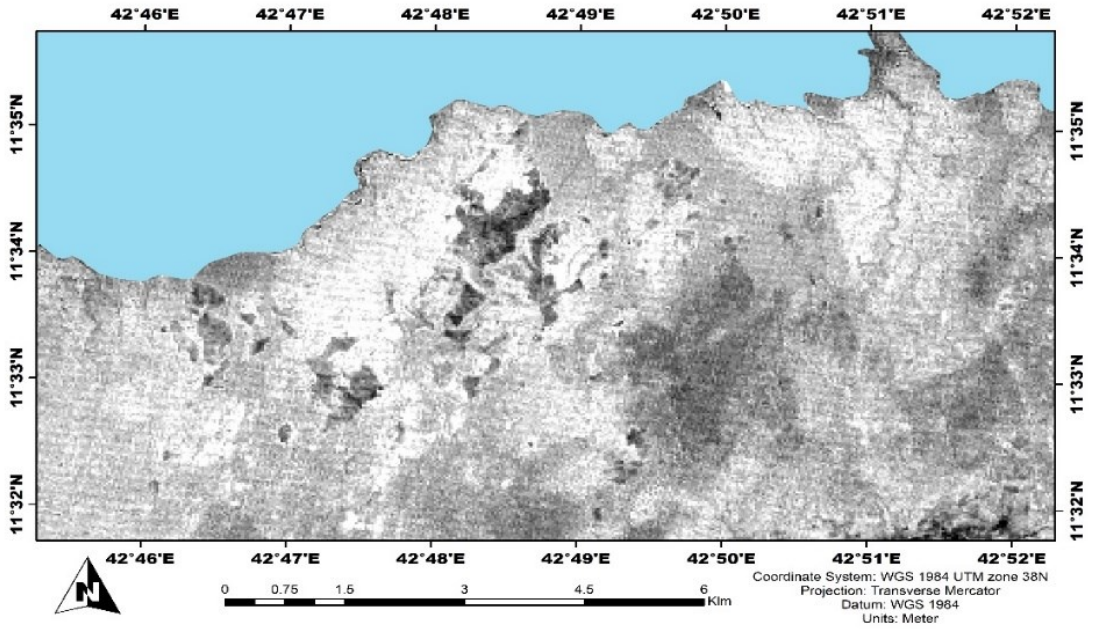


**Figure 5: ASTER band ratio (b4/b2): Iron oxide appears bright pixel.**

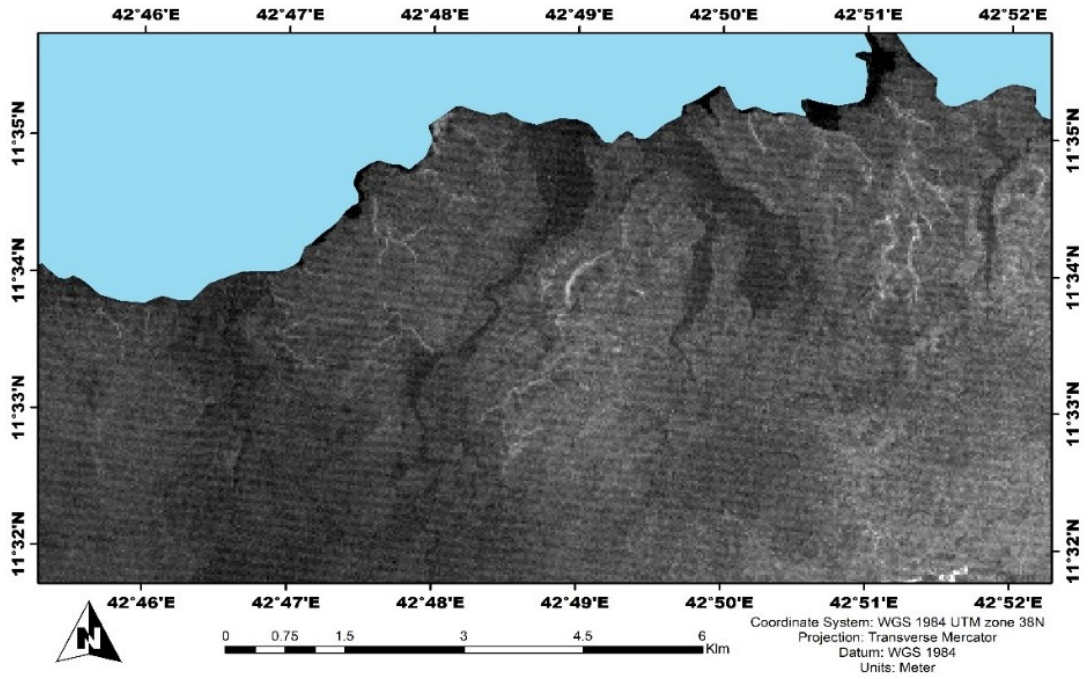


**Figure 6: ASTER band ratio (b3/b2): Vegetation appears bright pixel.**

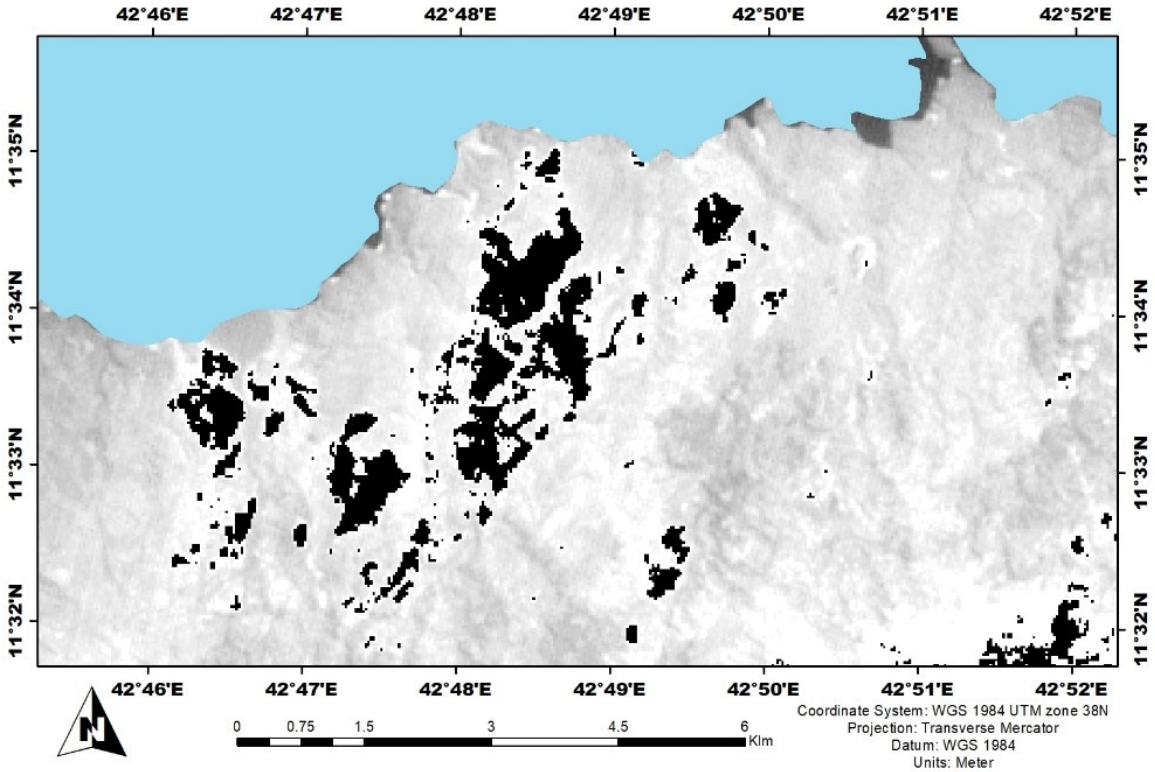


**Figure 7: ASTER band ratio ((b4*b7)/(b6*b6)) and ( (b4*b7)/(b5*b5)) ): Hydroxyl and hydroxy appears dark pixel.**

**5.1. Principal compound analysis.**

The principal compound analysis (table 2) were displayed to get the eigenvector matrix from the original data of nine bands.PC 1 present negative loading in band 1, band 2 and band 3 and positive loading in band 4 to band 9 (Figure 8) .PC1 indicated probably the difference between VNIR subsystem and SWIR subsystem (Pour et al.,2011).PC 2 has negative loading band 5 (-0.019877) and positive loading in band 4(0.067119) ,band 6 (0.098094) and band 7(0.011507) there for the OH bearing is showing bright pixel. On the other hand, PC 3 presents the inverse of PC 2, that why the OH mineral distribution as dark pixel. PC 4 show us positive loading in band 5, band 6 and band 7 which can emphases the alteration mineral mainly came from AL (OH) such as alunite, kaolinite and illite. Those minerals present high absorption of the wavelength between (2.14 µm -2.28 µm) which represent a bright pixel in the image PC4 (Crosta and Moore (1989) and Loughlin (1991)).On the other hand, the negative loading of band 8 and band 9 indicated the mineral that content mainly Fe and Mg (OH) because those mineral have absorption wavelength between (2.29 µm and 2.43 µm) such as tremolite, carbonate, calcite, and dolomite. Those minerals show us a dark pixel.PC 5 has negative loading band 8 (-0007439) and positive loading band 9 (0.008474) which show the Fe and Mg (OH) with a bright pixel. The Fe and Mg (OH) can indicate the propylitic alteration such as Chlorite, Epidote and calcite. PC 6 presents the inverse of PC5 due to the positive loading band 8 (0.004739) and negative loading band 9 (-0.010391) with dark pixel for the propylitic distribution.PC 7 emphases the distribution of iron oxide with negative loading band 2 (-0.008769) and positive loading band 4 (0.006414). The iron oxide appears as a bright pixel because of high absorption in band 2 and high reflectance in band 4 (Velosky et al., 2003).PC 8 has positive loading in band 2 (0.003761) and negative loading band 3 (-0.002182) due to high reflectance of band 3 and low reflectance band 2 (Xu et al., 2004). The distribution of vegetation appears bright pixel. PC 9 seems noisy and did not show any information. Figure 8 show the color composite RGB of PC4 (Al (OH)),PC 6 (fe,Mg(OH)) and PC 7(iron oxide) bearing mineral. This color composite was generated to show the distribution of iron oxide and the hydrothermal alteration in the study area. The area are displays by four main color; red (advanced argillic ,phyllic alteration), yellow (advanced argillic ,phyllic and propylitic alteration),green (propylitic alteration), and blue (iron oxide) (figure 9)

**Table 2: Eigenvector matrix of principal components analysis on VNIR+SWIR bands of ASTER data for Arta area (Blue color indicate the absorption and grey color indicate the reflectance).**

| Eigenvector | PC 1 | PC 2 | PC 3 | PC 4 | PC 5 | PC 6 | PC 7 | PC 8 | PC 9 |
|---|---|---|---|---|---|---|---|---|---|
| Band 1 | -0.982034 | -0.136468 | 0.105437 | 0.074874 | 0.005619 | 0.014602 | 0.001922 | 0.003586 | 0.000632 |
| Band 2 | -0.060702 | 0.828207 | 0.551517 | -0.05481 | 0.021659 | -0.051504 | -0.008769 | 0.003761 | 0.000766 |
| Band 3 | -0.16922 | 0.529886 | -0.821623 | -0.085327 | -0.087109 | -0.024838 | 0.005618 | -0.002182 | -0.000557 |
| Band 4 | 0.028081 | 0.067119 | -0.092336 | 0.629261 | 0.698981 | -0.31812 | 0.006414 | 0.018531 | -0.007232 |
| Band 5 | 0.021166 | -0.019877 | 0.031958 | 0.374377 | -0.637725 | -0.671497 | 0.018006 | 0.007226 | -0.000122 |
| Band 6 | 0.044941 | 0.098094 | -0.000928 | 0.658466 | -0.305592 | 0.660273 | 0.157483 | 0.023202 | 0.009623 |
| Band 7 | 0.005229 | 0.011507 | -0.009268 | 0.118371 | -0.055958 | 0.091196 | -0.982677 | -0.09018 | 0.022529 |
| Band 8 | 0.002116 | -0.003719 | -0.003452 | -0.018813 | -0.007439 | 0.004739 | -0.094439 | 0.991165 | -0.090614 |
| Band 9 | 0.000422 | -0.001316 | -0.001714 | -0.006192 | 0.008474 | -0.010391 | 0.012177 | 0.09216 | 0.995558 |

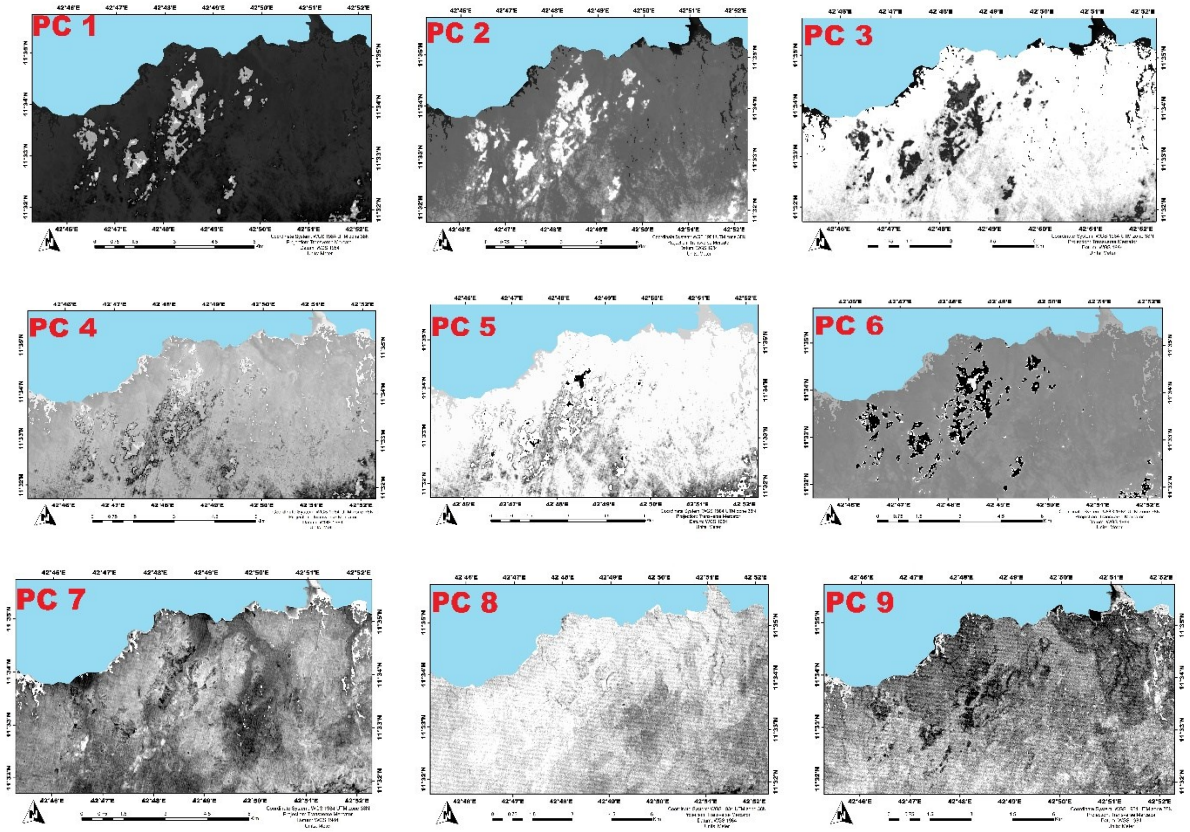


**Figure 8: Result of principal compound analysis.**

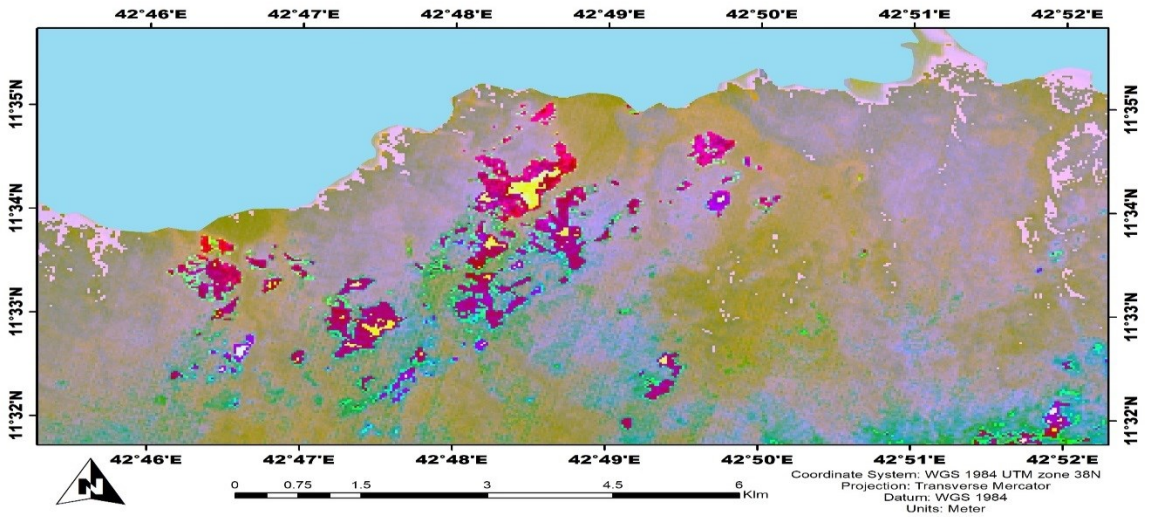


**Figure 9: ASTER false color image (R:G:B =PC4:PC6:PC7), Red (advanced argillic ,phyllic alteration), Yellow (advanced argillic ,phyllic and propylitic alteration),Green (propylitic alteration), and blue (iron oxide).**

## 6. CONCLUSION

The subsystem VNIR and SWIR of ASTER image have been successfully identify the hydrothermal alteration related in the Arta area. The color composite, band ratio and principal compound analysis have been well determined the distribution of altered mineral. The true color composite, the band ratio (b3/b2) and PC 8 were correctly detected the distribution of vegetation. The band ratio (b4/b2) and PC7 have been well performed for the detection of Iron oxide. The false-color composite image RGB (B4, B6, B8), has clearly show the distribution of advanced argillic (alunite, kaolinite), phyllic alteration (illite, montmorillonite) and Propylitic alteration (Chlorite, Epidote, and Calcite ).Base on PC4 and PC 5,the mineral content Al(OH) ,Fe and Mg(OH) have been highlight. The distribution of hydroxyl bearing has been done correctly which shown the same result of PC2 and PC3. The result are verified via color composite of principal compound analysis which has confirmed the alteration area fund during the

previous method. According to the result, the alterations are located in the Rhyolite intrusion (OH bearing) surrounded by iron oxide. The alteration mineral could be caused by the Rhyolite intrusion.

**REFERENCES**


Abrams, M., The Advanced Spaceborne Thermal Emission And Reflection Radiometer (ASTER): Data products for the high spatial resolution imager on NASA's Terra platform: International Journal of Remote Sensing, v. 21, p. 847–859, 2000.

Amin B P and Mazlan H 2011 *Journal of Asian Earth Sciences* **42** 1309–1323, 2011

Crowley, J.K., Brickley, D.W., and Rowan, L.C. "Airbone imaging spectrometer data of the Ruby Mountains, Montana: Mineral discrimination using relative absorption band-depth images": Remote Sensing of Environment, 1989.

Crósta, A.P., Moore, M.J.,. Enhancement of Landsat Thematic Mapper Imagery for Residual Soil Mapping in SW Minas Gerais State Brazil: A Prospecting Case History in Greenstone Belt Terrain. In: 9th Thematic Conference on Remote Sensing for Exploration Geology, Calgary, 1173–1187, 1989.

*et al.*, "Radiometric Calibration of ASTER Data," *J. Remote Sens. Soc. Japan*, vol. 15, no. 2, pp. 108–115, 1995.

"International Journal of The Advanced Spaceborne Thermal Emission and Reflection Radiometer ( ASTER ): Data products for the high spatial resolution imager on NASA ' s Terra platform," no. August 2013, pp. 37–41, 2010.

L. C. Rowan and J. C. Mars, "Lithologic mapping in the Mountain Pass , California area using Advanced Spaceborne Thermal Emission and Reflection Radiometer ( ASTER ) data," vol. 84, pp. 350–366, 2003.

Q. Li, B. Zhang, L. Lu, and Q. Lin, "Hydrothermal alteration mapping using ASTER data in Baogutu porphyry deposit, China," *IOP Conf. Ser. Earth Environ. Sci.*, vol. 17, no. 1, 2014.

Pour, B.A., Hashim, M., Marghany, M., 2011. Using spectral mapping techniques on short wave infrared bands of ASTER remote sensing data for alteration mineral mapping in SE Iran. Int. J. Phys. Sci. 6 (4), 917–929, 2011.

"Principal component analysis for alteration mapping," *Photogramm. Eng. Remote Sens.*, vol. 57, no. 9, pp. 1163–1169, 1991.

Q. Li, B. Zhang, L. Lu, and Q. Lin, "Hydrothermal alteration mapping using ASTER data in Baogutu porphyry deposit, China," *IOP Conf. Ser. Earth Environ. Sci.*, vol. 17, no. 1, 2014.

Rowan, L.C., Hook, S.J., Abrams, M.J., and Mars, J.C. "Mapping hydrothermally altered rocks at Cuprite, Nevada, using the Advanced Spaceborne Thermal Emission and Reflection Radiometer" (ASTER), A new satellite-imaging system: Economic Geology and the Bulletin of the Society of Economic Geologists,v. 98, p. 1019–1027, , 2003.

Rowan, L.C., and Mars, J.C. Lithological mapping in the Mountain Pass, California area using Advanced Spaceborne Thermal Emission and Reflection Radiometer (ASTER) data: Remote Sensing of Environment, 2003, v. 84, p. 350–366, 2003.

S. I. J. H. Ook, M. I. J. A. Brams, U. S. G. Survey, and M. Stop-, "SCIENTIFIC COMMUNICATIONS," vol. 98, no. December 1999, pp. 1019–1027, 2003.

Singh, A., Harrison, A.,. Standardized principal components. International Journal of Remote Sensing 6, 883–896, 1985.

Volesky, J.C., Stern, R.J., Johnson, P.R.. Geological control of massive sulfide mineralization in the NeoproterozoicWadiBidah shear zone, southwestern Saudi Arabia, inferences from orbital remote sensing and field studies. Precambr. Res. 123, 2003

Y. Ninomiya, "Lithologic mapping with multispectral ASTER TIR and SWIR data," *Sensors, Syst. Next-Generation Satell. VII*, vol. 5234, no. February 2004, p. 180, 2004.

Yongming Xu, Qizhong Lin, Yun Shao, and Lu Wang, "Extraction mechanism of alteration zones using ASTER imagery," *IGARSS 2004. 2004 IEEE Int. Geosci. Remote Sens. Symp.*, vol. 6, no. c, pp. 4174–4175, 2004.

Y. Yamaguchi, A. B. Kahle, H. Tsu, T. Kawakami, and M. Pniel, "Overview of advanced spaceborne thermal emission and reflection radiometer (ASTER)," *IEEE Trans. Geosci. Remote Sens.*, vol. 36, no. 4, pp. 1062–1071, 1998.

Yamaguchi, Y., Kahle, A.B., Tsu, H., Kawakami, T., and Pniel, M., "Overview of Advanced Spaceborne Thermal Emission and Reflection Radiometer" (ASTER): IEEE Transactions on Geoscience and Remote Sensing, v. 36, p. 1062–1071, 1998.



Y. Ninomiya, "Lithologic mapping with multispectral ASTER TIR and SWIR data," *Sensors, Syst. Next-Generation Satell. VII*, vol. 5234, no. February 2004, p. 180, 2004.

Yongming Xu, Qizhong Lin, Yun Shao, and Lu Wang, "Extraction mechanism of alteration zones using ASTER imagery," *IGARSS 2004. 2004 IEEE Int. Geosci. Remote Sens. Symp.*, vol. 6, no. c, pp. 4174–4175, 2004.

Y. Yamaguchi, A. B. Kahle, H. Tsu, T. Kawakami, and M. Pniel, "Overview of advanced spaceborne thermal emission and reflection radiometer (ASTER)," *IEEE Trans. Geosci. Remote Sens.*, vol. 36, no. 4, pp. 1062–1071, 1998.